Nanoscale Advances

Accepted Manuscript

This article can be cited before page numbers have been issued, to do this please use: S. K B and K. Suvardhan, *Nanoscale Adv.*, 2025, DOI: 10.1039/D5NA00633C.

ROYAL SOCIETY OF CHEMISTRY

rsc.li/nanoscale-advances

A hierarchically porous RhB encapsulated ZIF-7 as a dual emission fluorescence probe for ultrasensitive detection of melamine in infant formulations

Sreevidhya K B, Suvardhan Kanchi*

*Department of Chemistry, CHRIST University, Bengaluru 560029, India
*Centre for Renewable Energy and Environmental Sustainability, CHRIST University, Bengaluru 560 029, India

Abstract

Melamine is an unauthorized food additive, a highly concerning adulterant in foods that can either occur accidentally or intentionally in dairy products, with potential health risks on exposure to higher concentrations. An ultrasensitive fluorescent probe based on the dual emissive RhB_x@ZIF-7 was developed to detect melamine. In this work, a fluorescent dye, Rhodamine B (RhB), is successfully encapsulated into metal-organic framework (MOF) pores of ZIF-7 to form a fluorescent probe (RhB_{30}@ZIF-7), with dual emission properties to enable the detection of melamine at low concentrations. RhB_{30}@ZIF-7 was optimized by varying experimental parameters including temperature (25°C), pH (7.0), incubation time (10 min), and probe concentration (1 mg/ml) to enhance the sensitivity and selectivity. The observed fluorescent quenching towards melamine was primarily attributed to the mechanisms of internal filtering effect (IFE), due to the absorption of excitation wavelength by melamine, causing a turn-off response in the system. The limits of detection (LOD) and limits of quantification (LOQ) were found to be 0.47 µM and 1.4 µM, respectively, with R^2 of 0.99. The current study reveals the enhanced fluorescence of RhB_{30}@ZIF-7, which has not been explored yet, and the intermolecular interaction of RhB and ZIF-7 contributing to fluorescence sensing, paving the way for the monitoring of food safety.

Keywords: ZIF-7, RhB, melamine, dual emission, fluorescent probe, infant formulations

---

**Corresponding Author: suvardhan.k@christuniversity.in (S Kanchi)*

View Article Online
DOI: 10.1039/D5NA00633C

1. Introduction

Melamine (2,4,6-triamino-1,3,5-triazine) is an industrially attractive compound, extensively used in the molding of plastics with formaldehyde, manufacturing of cookware, plastic crockery, adhesives, and as a fertilizer additive [1, 2]. It is also utilized as a pharmaceutical drug carrier. The nitrogen richness in melamine (66% nitrogen by mass) leads to its illegal usage in the food industry, as it gives properties of protein to the food composition. Thus, melamine is profoundly adulterated in dairy products, infant formulations, milk, livestock feed, and a range of protein-rich diets by unethical manufacturers, to falsely inflate the protein level to an unusual amount owing to its low cost and ability to mimic analytical protein characteristics in standard Kjeldahl and Dumas tests [3-5]. The adulteration of food products using harmful chemicals/substances can pose an elevated risk to consumer health, urging the efficient and continuous monitoring of toxins and chemicals in food matrices. Melamine has not been authorized as a food additive in the Codex Alimentarius Commission (CAC) and national authorities, and is listed as a hazard if inhaled, ingested, or skin exposure [6]. Chronic exposure to melamine can cause cancer or kidney damage [2]. The World Health Organization's (WHO) International Agency for Research on Cancer has placed melamine on the list of 2B carcinogens in 2012 because of its ability to cause harm to human health [6]. The US Food and Drug Administration (FDA) recommended the safety limit of melamine that should be present in adult food and infant formulations as 2.5 mg/kg and 1 mg/kg concentrations, respectively[2]. Intake of more than the permitted amount of melamine can lead to the development of insoluble crystals of melamine cyanurate in the kidneys, tissue damage, as well as acute kidney failure in humans and animals, which is potentially fatal [7, 8]. Melamine in high concentrations can cause food poisoning, especially in children and infants, therefore the WHO has established a tolerable daily intake (TDI) at 0.2 mg kg^{-1} of body weight per day for humans based on CAC [9]. The severe health implications caused by melamine adulteration

View Article Online
DOI: 10.1039/D5NA00633C

across all age groups and animals necessitate the development of a selective and sensitive sensor for its detection in dairy products and food.

To date, several approaches have been used to analyze melamine involving high performance liquid chromatography (HPLC)[10], liquid chromatography/tandem mass spectrometry (LC/MS)[11], gas chromatography-mass spectrometry (GC-MS)[12, 13], electrophoresis[14], immune assay analysis (ELISA- Enzyme-Linked Immunosorbent Assay)[15, 16], surface-enhanced Raman spectroscopy (SERS)[17] and electrochemical sensing[18, 19]. Despite the selectivity and sensitivity of these methods, their practical implementation in regular analysis is limited by the costly equipment, complex sample pretreatment, skilled manpower, complicated operation, and use of chemical solvents[20]. Over the past decade, sensor technologies have been increasingly recognized to supplement traditional instrumentation analysis for detecting contaminants/adulterants in dairy products[21-23]. Optical sensors are often rapid, efficient, cost-effective, user-friendly, and sensitive to a certain extent for the detection of adulterants in a wide range of complex matrices[24]. However, the developed probe's sensitivity and selectivity remain challenging. Therefore, to address the sensitivity and selectivity, it is highly essential to develop new probes using mesoporous self-assembly structures. Among these, metal-organic frameworks (MOFs) are progressively being investigated for their potential in detecting chemical contaminants in food products, including dairy products. Metal organic frameworks (MOFs) are hybrid crystals consisting of an inorganic framework and organic building blocks. Furthermore, advancements have been made in improving the physicochemical properties of MOF-based sensors by post-synthetic modifications such as doping, encapsulation, surface functionalization, and defect engineering[25]. Luminescent metal organic frameworks have recently attracted significant attention due to their structural and chemical benefits, including high surface area, luminescent modes, and quick response time [26].

View Article Online
DOI: 10.1039/D5NA00633C

A dual emission fluorescent platform was developed for the sensing and quantification of melamine in milk powder over a wide range of concentration using Tb@NH_2-MIL-253 (Al) MOF as a fluorescent probe with low LODs of 40 nM [20]. Similarly, a nanocomposite of Ag – MOFs doped with magnetic nanocatalyst for sensing of melamine with simple visualization showed LOD of 1.8 ppm with a recovery of 77% [27]. In another study, both Hg^+ and melamine were detected using CeO_2 incorporated MIL(Fe) via colorimetric detection. The CeO_2-MIL(Fe) composite showed a peroxidase–like activity for melamine and achieved LODs of 8 nM [28]. The nano-ceria encapsulated MOF, CeO_2@NH_2-MIL(Fe) based fluorescent biosensor was reported for the detection of melamine and Pb^{2+} with a LOD of 7.6 nM and 1.3 nM, respectively, using a hybridization chain reaction amplification strategy [29]. A method in which ZIF-8 was confined with highly luminescent perovskite quantum dots ($CsPbBr_3$) via a two-step *in-situ* growth method to detect Cu^{2+} and melamine showed LODs of 2.64 nM and 4.66 nM, respectively. This sensor exhibited an "on-off-on" mechanism by implementing the quenching property of Cu^{2+} on $CsPbBr_3$/HZIF-8, which was then restored by competitive adsorption by the amine group in melamine[30]. The Zr-based MOF was reported as a ratiometric fluorescent probe for sensing melamine with a LOD of 90 nM. UiO-66 was encapsulated with tris(2,2-bipyridyl)ruthenium(II)chloride hexahydrate ($[Ru(bpy)_3]^{2+}$) via the solvothermal method to achieve dual-emission fluorescent probe[31]. MOFs encapsulated with metals, nanoparticles, and dyes have been studied for the detection of melamine, while the combination of RhB_{30}@ZIF-7 has not been explored.

MOFs with zeolitic architectures, also known as Zeolitic imidazolate frameworks (ZIFs), a subfamily of MOFs, are one of the significant research areas due to their combination of properties from both MOFs and zeolites [32]. ZIFs have zeolite framework topologies with transition metals occupying tetrahedral positions and imidazolate units as bridging ones, resulting in high surface area, micro porosity, and superior chemical and thermal stability [33,

View Article Online
DOI: 10.1039/D5NA00633C

[34]. The majority of ZIFs have inherent luminescence either by virtue of the metal nodes themselves or the organic ligands that link them together, which features only a single emission with low stability and sensitivity. On the other hand, fluorescence as a result of incorporated guest molecules significantly contributes to highly efficient fluorescence-based sensing[35]. ZIF-7 is a well-known MOF candidate in the ZIF family of MOFs with two porous pockets in a single porous capsular shell, discovered by Huang et al. in 2003[36]. When integrated with fluorescent molecules, their unique luminescent properties are enhanced, gaining traction in the realm of optical sensing[23]. Inherent luminescence combined with a fluorescent guest molecule can form a dual emission system with improved luminescence performance[37-41].

In the current work, a guest@MOF approach utilizes the porous nature of MOFs as a 'host' to confine fluorescent molecules as 'guest' within the extended MOF structures for optical sensing applications[42, 43]. Dyes are ideal guests for the use in guest@MOF systems[44] as the majority of this kind do not emit fluorescence in the solid state due to aggregation-caused quenching(ACQ)[45, 46]. Dye monomers separated via encapsulation into MOF pores can induce fluorescence while existing in the solid state and are durable over time[47-50]. Rhodamine-B (RhB) is a cationic dye having high PLQY and stability[51]. RhB has been included in MOFs such as ZIF-71[52], Zr-MOF[53], ZIF-8[4], Co MOF[54], ZIF-7 III Metal organic nanosheets[55], Zn MOF[56], Eu(BTC)[57], for the detection of cations, nitro explosives, pesticides, extraction of different phenols, detection of phenolic compounds in food, volatile organic compounds, or picric acid, respectively.

Rhodamine-B was chosen as the guest molecule for the ZIF-7 framework due to its structural compatibility. It is a planar molecule where, Ph-COOH moiety is located perpendicular to the molecular plane of the xanthane backbone. Thus, it is favourable for encapsulation within pockets of host ZIF-7. A careful investigation of host structure revealed a pocket of 17.34 ×

View Article Online
DOI: 10.1039/D5NA00633C

11.47 Å with an entry of 6.31 × 4.79 Å. The dimensions of guest species (16.19 × 12.83 × 6.97 Å)[47] for RB are comparable to the host dimensions; hence, it is apparent that ZIF-7 to accommodate a guest Rhodamine-B within its pockets. The important reason behind the selection of Rhodamine-B as a guest species lies within its interesting fragments and switch-on/switch-off states of fluorescence. On the other hand, an exact match of the pore metrics and aromatic backbone of benzimidazole is advantageous to opt for ZIF-7 as a host material, as shown in Figure 1. The encapsulation study was attempted by in situ encapsulation. Efforts for controlling fluorescence states of guest species in the confined environment of ZIF-7 resulted in an exciting series of host-guest compounds, accompanied by exciting fluorescence properties.

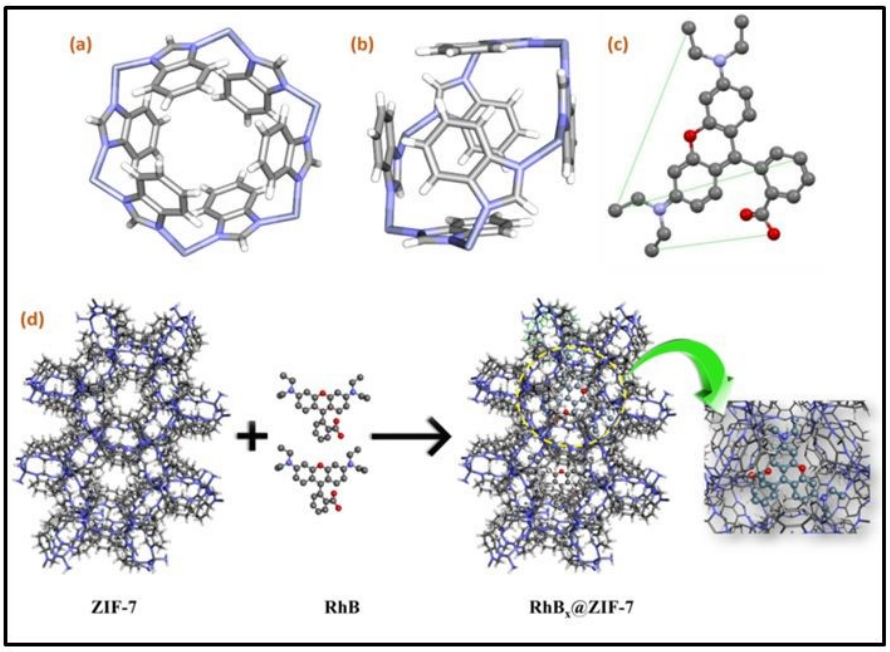

Figure 1. Illustration of ZIF-7 structure in two different orientations (a,b) and RhB with molecular dimensions (c). Schematic representation of RhB occupying pores of ZIF-7 (d).

2. Experimental

2.1. Instrumentation

The crystal structure of MOF and its composites was studied using a Powder X-ray diffractometer (Rigaku Mini Flex600 XRD, USA), Cu Kα radiation at 25°C. The optical

View Article Online
DOI: 10.1039/D5NA00633C

studies were investigated using a UV Spectrophotometer (Shimadzu UV–1800) and spectrofluorophotometer (Shimadzu RF-6000), recorded at room temperature. Functional group determination of composites was performed using a Fourier transform infrared (FTIR) spectrometer (Shimadzu-A224056, Japan). The functional groups present in the composites were characterized by a Fourier- and Raman microscopy (Renishaw Raman inVia Confocal microscope, UK). The scanning electron microscopy (APREO2, USA) was used for surface morphology analysis. Thermal stability was investigated using a TGA/DTA Analyzer (NETZSCH, NJA – STA 2500 Regulus).

2.2. Chemicals and reagents

Zinc nitrate [$(Zn(NO_3)_2 \cdot 6H_2O)$,98%], *N, N'*-Dimethylformamide [DMF,99%], Acetone [$(CH_3)_2CO$, 99%], Triethylamine [NEt_3, 98%], and Rhodamine-B [RhB] were purchased from Avra Synthesis Pvt.Ltd, Telangana, India. Benzimidazole [BIm, $C_7H_6N_2$] was purchased from Spectrochem Pvt., Ltd., Mumbai, India. Ultra-pure deionized water collected from the Milli-Q (IQ 7000) ultrapure water purification system. All the chemicals were received and used as such without further purification.

2.3. Synthesis of pristine ZIF-7

0.75 mM $Zn(NO_3)_2 \cdot 6H_2O$ was dissolved in 5 ml of DMF taken in a 15 ml glass vial to get solution A. 1.87 mM BIm was dissolved in 5 ml of DMF taken in another 15 ml glass vial. Add 1.87 mM NEt_3 and ultrasonicate to get solution B. Mix solutions A and B in a 50 ml conical flask and stir well at 300 rpm for 30 min to get white precipitate. The precipitate was washed with DMF and acetone three times, followed by drying at a temperature of 60 °C for 24 h to obtain white crystals.

2.4. In-situ synthesis of RhB_x@ZIF-7

0.75 mM $Zn(NO_3)_2 \cdot 6H_2O$ was dissolved in 5 ml of DMF taken in a 15 ml glass vial to get solution A. 1.87 mM BIm was dissolved in 5 ml of DMF taken in another 15 ml glass vial. Add 1.87 mM NEt_3 and ultrasonicate to get solution B. Mix solutions A and B in a 50 ml

View Article Online
DOI: 10.1039/D5NA00633C

conical flask. Then, add different amounts of RhB (10, 30, 50 mg) to the conical flask and stir at 250 rpm for 30 min, resulting in the formation of pink precipitates, RhB_x@ZIF-7 (x=10,30,50). The products were subjected to multiple washes with DMF and acetone till the pink colour disappeared from the supernatant solution. The pink precipitate was dried at 60°C for 24 h to obtain the crystals for further use (Figure 2).

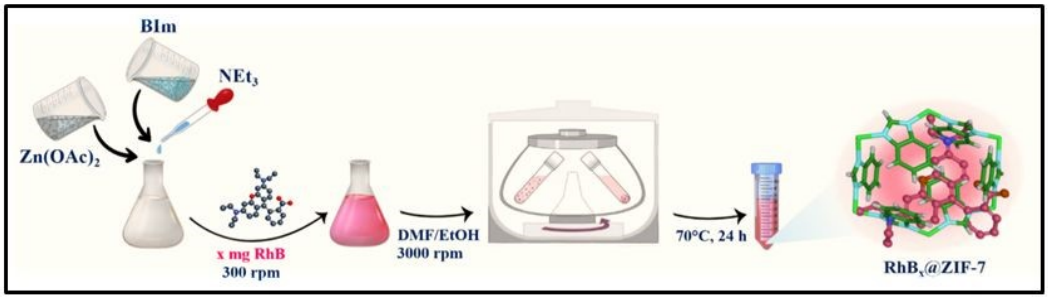

Figure 2. Schematic illustration of synthesized RhB_x@ZIF-7.

3. Results and discussion

3.1. Characterization of ZIF-7 and RhB_x@ZIF-7

Raman spectrum of pristine ZIF-7 (Figure 3a) showed a sharp peak at 120 cm^{-1} associated with the lattice modes of vibration, along with the vibrational modes associated with the metal ligand interaction between zinc and benzimidazole nitrogen atoms. The peaks corresponding to bending modes of vibrations of the entire framework appeared at lower wavenumbers between 200 – 800 cm^{-1}, and those corresponding to the vibrations of intra-framework bonds were found at 800-1600 cm^{-1} range, as expected [58]. A primary peak at 500 cm^{-1} was characteristic of the symmetric stretching of the imidazole ring in ZIF-7, along with a bending vibration mode of the imidazole ring at 645 cm^{-1}. The N-H & C-H vibration of imidazolate and benzene ring with π-conjugation and aromatic property was supported by the peak around 1590 cm^{-1}. A peak at 3000-3100 cm^{-1} showed aromatic C-H stretching vibrations of the benzene ring, while the aliphatic C-H stretching vibrations were observed around 2800- 3000 cm^{-1} [59].

View Article Online
DOI: 10.1039/D5NA00633C

The XRD pattern of as-synthesized RhB_x@ZIF-7 reveals the efficient inclusion of RhB into ZIF-7, retaining its crystallinity without framework disruption. The characteristic peaks of ZIF-7 match its simulated XRD pattern, as shown in Figure 3b. The diffractogram revealed peaks at 2θ values 7.2°, 7.6°, 10.0°, 14.3°, 15.4°, 16.2°, 18.5°, and 20.4° assigned to the specific miller indices (101), (110), (021), (202), (220), (122), (113), and (140) respectively confirms crystallinity and purity of synthesized pristine ZIF-7 (CCDC deposition no– 602541). The appearance of sharp peaks indicates its sodalite (SOD) topology and cubic crystal structure. The diffractogram of RhB_x@ZIF-7 retained characteristic peaks at 2θ values 7.2°, 7.8°, 10.0°, 14.9°, 15.7°, 16.2°, 18.5°, and 20.4° indicating structural integrity of the framework. Distinct peaks of RhB is also visible at 2θ values 9.2°, 11.3°, 12.8°, 14.6°, 16.1°, 16.7°, and 18.5° corresponding to specific miller indices (002), (020), (112), (022), (122), (113), and (004) respectively (CCDC deposition no– 1160674)[60], confirmed the successful encapsulation of RhB into ZIF-7 with individual crystallinity intact. The introduction of RhB into the pores of ZIF-7, the unit cell parameters are slightly disturbed causing a change in the intensity and 2θ values in XRD pattern [47]. Further, the typical patterns in the composite RhB_{30}@ZIF-7 are more in agreement with the aforementioned values.

Figure 3c depicts the FTIR spectra of the synthesized pristine ZIF-7 and RhB_x@ZIF-7 composites analyzed in the range of 4000-300 cm^{-1} at room temperature. The stretching vibration of the C-N bond contributes to a characteristic sharp peak at 1640 cm^{-1}. All the samples give peaks at 1470 cm^{-1} and 748 cm^{-1} corresponding to C-C vibrations and C-H vibrations in the benzimidazole ligand of ZIF-7. The peaks between 420-647 cm^{-1} represent the Zn-N bond in ZIF-7 [61]. A decrease in intensity of peaks between 600 cm^{-1} and 450 cm^{-1} corresponds to the non-covalent interaction between the hydroxyl group of RhB and nitrogen of the imidazolate ring, and a similar characteristic peak of RhB was also observed in the same wavenumber range at 600 cm^{-1} and 450 cm^{-1}[52]. The FTIR spectra of synthesized ZIF-7 and RhB_x@ZIF-7 composites showed a similar trend in peak positions, indicating structural

View Article Online
DOI: 10.1039/D5NA00633C

similarity across all four samples. The obtained results suggest the encapsulation of RhB into the ZIF-7 rather than adsorption onto its surface.

Thermogravimetric analysis (TGA) of pristine ZIF-7 and RhB_x@ZIF-7 composites showed weight loss due to non-coordinated and coordinated water molecules below 200 °C (ca. 6 wt%) as shown in Figure 3d. Further weight loss observed below 300 °C indicates the decomposition of unreacted nitrates from the precursors and residual solvents trapped inside the framework (ca. 11 wt%) [62]. The weight loss at temperatures between 300 °C - 400 °C for RhB_x@ZIF-7 was attributed to the thermal degradation and destruction of encapsulated RhB (ca. 2 wt%) [57]. The breakdown of the xanthene core of RhB leads to the formation of small organic fragments at 300°C, and complete oxidation occurs at 400°C, resulting in carbonaceous residue. Among all the RhB_x@ZIF-7 (x=10, 30, 50), the least solvent evaporation was observed in RhB_{30}@ZIF-7. The frameworks collapsed at temperatures above 500°C, with a pronounced weight loss observed for all RhB_x@ZIF-7 samples and ZIF-7 (ca. 40 wt%) [34]. Finally, a stable combustion product, ZnO, is obtained by complete degradation for all the samples.

In order to ensure the encapsulation of RhB molecules inside ZIF-7 pores rather than adsorbed onto its surface, controlled experiments were carried out. The synthesized RhB_x@ZIF-7 composites were immersed in doubly distilled deionized water, and RhB molecules were not released from the framework, giving a preliminary confirmation of RhB encapsulation into ZIF-7. To determine the content of loading RhB, the synthesized RhB_x@ZIF-7 composites were decomposed by acid hydrolysis followed by UV spectrophotometer analysis. The loading fraction of RhB in ZIF-7 is determined as 0%, 0.069%, 2.0% and 8.4 % for pristine ZIF-7, RhB_{10}@ZIF-7, RhB_{30}@ZIF-7, and RhB_{50}@ZIF-7, respectively (See Figure S1 and Table S1). All these results demonstrate the loading of RhB into the ZIF-7 framework rather than adsorbed onto its surface.

View Article Online
DOI: 10.1039/D5NA00633C

In order to ensure the encapsulation of RhB molecules inside ZIF-7 pores rather than adsorbed onto its surface, controlled experiments were carried out. The synthesized RhB_x@ZIF-7 composites were immersed in doubly distilled deionized water, and RhB molecules were not released from the framework, giving a preliminary confirmation of RhB encapsulation into ZIF-7. To determine the content of loading RhB, the synthesized RhB_x@ZIF-7 composites were decomposed by acid hydrolysis followed by UV spectrophotometer analysis. The loading fraction of RhB in ZIF-7 is determined as 0%, 0.069%, 2.0% and 8.4 % for pristine ZIF-7, RhB_{10}@ZIF-7, RhB_{30}@ZIF-7, and RhB_{50}@ZIF-7, respectively (See Figure S1 and Table S1). All these results demonstrate the loading of RhB into the ZIF-7 framework rather than adsorbed onto its surface.

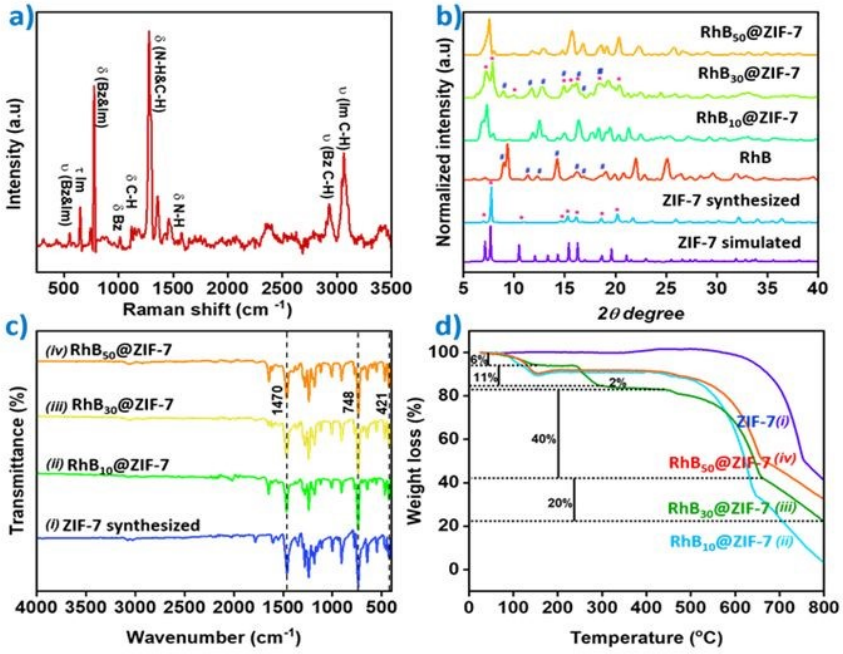

Figure 3. a) Raman spectra of pristine ZIF-7. b) The X-ray diffractogram showing crystalline structure of ZIF-7 simulated [CCDC deposition number 602541], pristine ZIF-7, RhB [CCDC deposition number 1160674], RhB_{10}@ZIF-7 v), RhB_{30}@ZIF-7, RhB_{50}@ZIF-7. c) FT-IR spectra of i) pristine ZIF-7 ii) RhB_{10}@ZIF-7 iii) RhB_{30}@ZIF-7 iv) RhB_{50}@ZIF-7. d) TGA curves of i) pristine ZIF-7 ii) RhB_{10}@ZIF-7 iii) RhB_{30}@ZIF-7 iv) RhB_{50}@ZIF-7.

View Article Online
DOI: 10.1039/D5NA00633C

The N_2 adsorption-desorption isotherms of pristine ZIF-7 and RhB_{30}@ZIF-7 were obtained at 77K, as shown in Figure 4. The BET surface area and pore volume measured for ZIF-7 are 1.27 m^2g^{-1} and 0.011 cm^3g^{-1} (Figure 4a). As suggested from previous reports, ZIF-7 is inaccessible to N_2 at 77K because of the narrow pore openings compared to the kinetic diameter of N_2[63]. The sample clearly shows complete blockage of the porosity up to a relative pressure of 0.8 with low adsorption capacity (0.61 mmol g^{-1}). After which, an increase in the amount of N_2 intake is observed due to the condensation of interparticle space[64]. For RhB_{30}@ZIF-7, the N_2 adsorption-desorption isotherms (Figure 4b) exhibit a different shape over the evaluated relative pressure range. The nitrogen adsorption is irreversible, with an amount of N_2 trapped at a low relative pressure of 0.23. The BET surface area and pore volume are 13.9 m^2g^{-1} and 0.028 cm^3g^{-1}. The increase in pore volume in RhB_{30}@ZIF-7 is due to the expansion of benzimidazole linkers that connect Zn metal clusters in the ZIF-7 framework to a porous structure when RhB is successfully encapsulated in its pores[65].

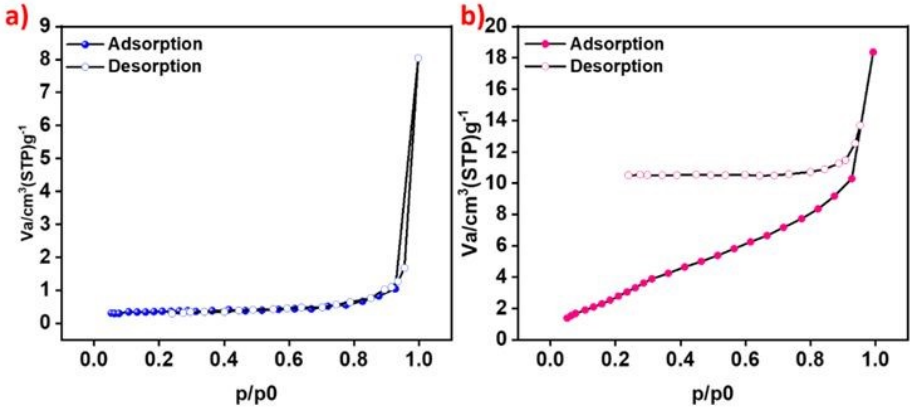

Figure 4: N_2 adsorption- desorption isotherms of a) pristine ZIF-7, b) RhB_{30}@ZIF-7.

The morphology of the ZIF-7, RhB_x@ZIF-7, and the effect of encapsulation was investigated using FE-SEM (Figure 5) along with elemental mapping to understand RhB distribution over ZIF-7 (See Figure S2-S5). The average particle size analysis is also determined using DLS analysis (See Figure S6). The images confirm the cubic crystalline structure[63] of ZIF-7 as shown in Figures 5a,b, with an average particle size distribution of 3.17 µm. RhB_{10}@ZIF-7

View Article Online
DOI: 10.1039/D5NA00633C

exhibited incomplete polyhedral structures of stacked nanosheet layers with stunted growth (Figures 5c,d) with an average size distribution of 1.26 µm. Flower-like structures consisting of rod-shaped particles with non-uniform distribution indicate the defective crystal growth of ZIF-7 in RhB_{10}@ZIF-7. SEM images of RhB_{30}@ZIF-7 at different magnifications in Figure 5e,f show a rhombic crystal structure[66] with an average particle size distribution of 1.3 µm. Compared to ZIF-7, RhB_{30}@ZIF-7 had a smaller crystal size. This change in morphology was attributed to the effect of RhB encapsulation that slows down the crystal growth of ZIF-7 at rhombohedral shape with truncated corners before attaining the final rhombic dodecahedral shape[9]. Faceted structures with soft edges were observed in SEM micrographs of RhB_{50}@ZIF-7 (Figure 5 g,h). The particles exhibited a uniform size with an average particle size distribution of 1.61 µm. It was evident from the SEM images that as the concentration of RhB increases, the particle size also increases, among which RhB_{50}@ZIF-7 showed the highest particle size and RhB_{30}@ZIF-7 showed well well-defined polyhedral shape compared with other RhB_x@ZIF-7 composites. All these evidences confirm that the composite RhB_{30}@ZIF-7 has RhB encapsulated into ZIF-7 without any change in the crystal morphology as expected for guest encapsulated ZIF-7. Incorporation of RhB_{30} to ZIF-7 enhances the fluorescence due to successful encapsulation into the pores of ZIF-7 compared to RhB_{10} and RhB_{50}. RhB in its solid state does not show emission due to aggregation-caused quenching (ACQ). However, when dispersed in a suitable medium (monomer separation), due to less aggregation, emission was enhanced. While RhB was introduced to ZIF-7, it was either adsorbed onto the framework surface or encapsulated inside the MOF pores. Adsorbed dye molecules were easily lost or removed while dispersing the RhB_x@ZIF-7 composite in water or other media where RhB was soluble, leaving behind the RhB molecules occupied inside the MOF pores intact. As the concentration of RhB added to the MOF increases, the concentration of RhB occupying the ZIF-7 pores also increases, causing a disrupted framework.

View Article Online
DOI: 10.1039/D5NA00633C

The change in unit cell parameters/ lattice parameters can be evident from the shape change from cubic to rhombic ZIF-7. Encapsulation of RhB into the pores decreases the pore availability, making it a rhombic MOF composite. Hardly one RhB molecule can be seated inside each pore of the framework due to its compatibility with the molecular size of RhB and the ZIF-7 pore structure. Such a separation of RhB molecules helps in reducing ACQ, thereby enhancing luminescence efficiency. Even though the composite exists in a solid state, the encapsulated RhB gives fluorescence property to the RhB_x@ZIF-7 composite.

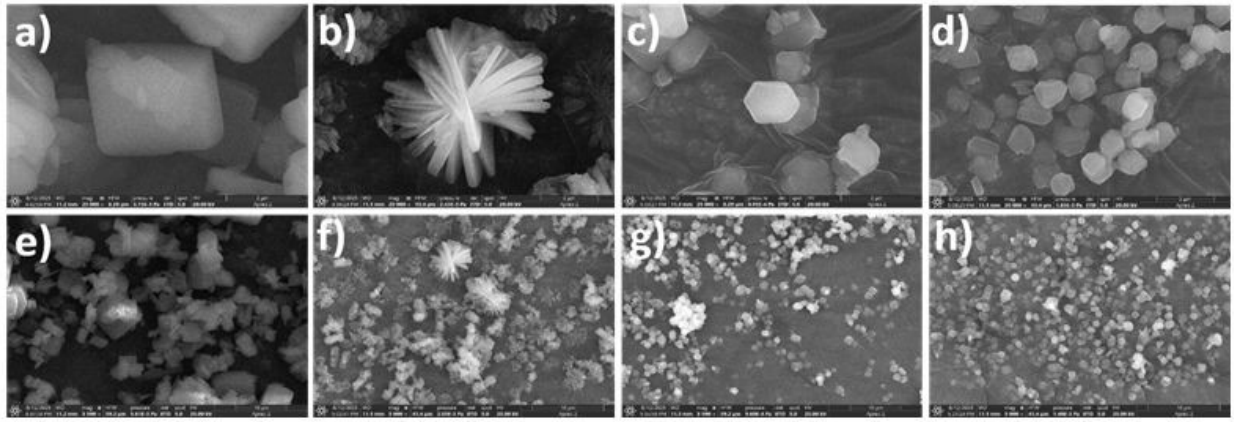

Figure 5: FE-SEM images of (a,b) pristine ZIF-7, (c,d) RhB_{10}@ZIF-7, (e,f) RhB_{30}@ZIF-7, and (g,h) RhB_{50}@ZIF-7.

3.2. Optical properties of ZIF-7 and RhB_{30}@ZIF-7

A UV-Visible spectrum of RhB, pristine ZIF-7, and RhBx@ZIF-7 is shown in Figure S7a. Pristine ZIF-7 showed absorption maximum at 243 nm, 271 nm, and 277 nm, which align with the reported values below 300 nm (between 200 to 300 nm). UV-Visible spectra of RhB show an absorption at a wavelength value of 554 nm [60]. The absorption maxima were shown at 242, 271, and 277 nm for RhB_{30}@ZIF-7. The presence of all the peaks corresponding to both the MOF and the absence of the absorption peak of the guest molecule, RhB, indicates successful encapsulation rather than adsorption.

The emission spectrum of ZIF-7 shows maximum intensity at 290 nm when excited at 271 nm, which was in agreement with the absorption spectra of ZIF-7 (Figure S7b). There was no

View Article Online
DOI: 10.1039/D5NA00633C

noticeable change in the emission wavelength of ZIF-7 when the excitation wavelength was changed. This type of behavior clearly depicts that the emission of ZIF-7 is independent of the excitation wavelength. The RhB_{30}@ZIF-7 shows dual emission at 290 nm and 578 nm, corresponding to both ZIF-7 and RhB, respectively, at λ_{ex} = 271 nm. At higher concentrations of RhB, the absorbance and emission were notable, whereas, not at the lower concentrations of RhB in RhB_x@ZIF-7. This behavior in absorption and emission intensity suggests new insights into the maximum incorporation of guest molecules into the MOF pores with a linear relation to the concentration of the guest molecule.

A comparison of the emission spectra at three different concentrations, 0.5, 1, and 2 mg/ml of ZIF-7, RhB_{10}@ZIF-7, RhB_{30}@ZIF-7, and RhB_{50}@ZIF-7 (λ_{ex}= 271 nm) separately is studied (Figure S7c). A distinct trend in emission intensity was observed across the samples. The emission intensity increases at 0.5 and 1 mg/ml, and decreases at 2 mg/ml, showing an irregular emission trend for ZIF-7, RhB_{10}@ZIF-7and RhB_{50}@ZIF-7. In contrast, RhB_{30}@ZIF-7 showed a continuous increase in emission intensity from 0.5 mg/ml to 1 mg/ml and 2 mg/ml, with maximum intensity shown at 2 mg/ml. The mixed trend in the intensity of ZIF-7, RhB_{10}@ZIF-7, and RhB_{50}@ZIF-7 was due to the inner filter effect that affects the intensity of emission with increasing concentration. However, for RhB_{30}@ZIF-7 inner filter effect was not observed as the intensity shows a regular response with concentration increase.

4. Method development for the detection of melamine

The fluorescence response of RhB_{30}@ZIF-7 with the addition of melamine was evaluated in aqueous solutions. The emission intensity of RhB_{30}@ZIF-7 varies with parameters such as pH, concentration of RhB_{30}@ZIF-7, incubation time, and temperature. The dual emissive system RhB_{30}@ZIF-7 showed emissions corresponding to both ZIF-7 and RhB at 290 nm and 578 nm, respectively, and both emissions were studied under different optimization

View Article Online
DOI: 10.1039/D5NA00633C

parameters. The sensitivity and selectivity of the system towards melamine detection were enhanced by studying the effect of pH, concentration of RhB_{30}@ZIF-7, incubation time, and temperature.

4.1. Effect of pH

Melamine, as a weak base, has a pKa value of 5.05, and the stability of RhB_{30}@ZIF-7 was affected by a change in pH. Therefore, the interaction between melamine and RhB_{30}@ZIF-7 was considerably affected by the pH of the sensing system. Further investigation on the effect of pH was performed by adjusting the pH of the solution, varying from 2.0 to 10.0, as shown in the supplementary information (Figure S8a). The PBS buffer, HCl, and NaOH were used to attain a specific pH for the desired reaction conditions. The 1 mg/ml RhB_{30}@ZIF-7 was added to each of the various pH solutions separately, along with the fixed concentration of melamine, and the emission spectra were recorded. The lowest intensity was observed at pH 7.0, whereas at pH levels less than 6.0 and above 8.0, the system showed high intensity due to framework rupture and release of RhB into the solution.

4.2. Effect of concentration

For the detection of melamine, solutions of RhB_{30}@ZIF-7 with a range of concentrations (0.5 mg/ml, 1 mg/ml, and 2 mg/ml) were added to separate beakers, and then 100 µl of 1.0 M melamine solution was added to each of the beakers. In each case, a noticeable change in fluorescence intensity was observed. After 10 min of mixing melamine and RhB_{30}@ZIF-7, the emission intensity is studied (Figure S8b). As the concentration of RhB_{30}@ZIF-7 increases from 0.5 mg/ml to 2.0 mg/ml, the detection efficiency is higher at 1.0 mg/ml. Therefore, 1 mg/ml of RhB_{30}@ZIF-7 was selected for further studies.

4.3. Effect of incubation time

During sensing studies, fluorescence measurements can be susceptible to incubation time after the addition of melamine into RhB_{30}@ZIF-7. The observations revealed that the incubation time was crucial for melamine detection. The effect of incubation time in

View Article Online
DOI: 10.1039/D5NA00633C

melamine detection was monitored; ranging from 0-20 min. 1 mg/ml RhB_{30}@ZIF-7 was added to 100 µl of 1.0 M melamine solution and kept for incubation while measuring the fluorescence intensity. The fluorescence intensity was measured at a specific time interval to identify the intensity variation with time. The emission intensity decreased steadily until it reached a lower maximum in 10 min. Then, after, emission intensity showed very little variation attributed to the maximum interaction between melamine and RhB_{30}@ZIF-7 as shown in the supplementary information (Figure S8c).

4.4. Effect of temperature

Hydrolysis of melamine can occur when the reaction conditions are changed. Therefore, the optimization of temperature in the detection of melamine is crucial. The effect of temperature was carried out from 20 °C-60 °C. 1 mg/mL RhB_{30}@ZIF-7 was added to 100 µl of 1.0 M melamine solution. The fluorescence quenching response was maximum at 30 °C (Figure S8d) when compared to other temperatures. The framework disruption and melamine hydrolysis to form cyanuric acid at high temperatures make it difficult to detect melamine at higher temperatures.

4.5. Performance of RhB_{30}@ZIF-7

100 mg of RhB_{30}@ZIF-7 was dispersed in 100 ml milli-Q water, and 100 µl of this solution was added to 1900 µl of doubly distilled ionized water and 1000 µl of PBS (pH 7.0) buffer to achieve the final concentration of 33.3 µg /mL. The standard solutions of melamine with varying concentrations were added to the RhB_{30}@ZIF-7 solution. The fluorescence emission spectra were recorded at λ_{ex}=271 nm after incubating the solution for 10 min at room temperature, as represented in Figure 6a. The selectivity of RhB_{30}@ZIF-7 towards melamine detection was further confirmed by the addition of possible interfering ions and chemicals in the presence of melamine.

4.6. Figures of merit

View Article Online
DOI: 10.1039/D5NA00633C

Limit of detection (LOD) and limit of quantification (LOQ) for the detection of melamine were determined using a plot of I_0/I v/s the concentration of melamine [M] (Figure 6b). The LOD and LOQ were calculated using equations (1) and (2), respectively. 'σ' is the standard deviation of the reaction at the minimum concentration, and 's' is the slope of the calibration curve [27, 28]. The Stern-Volmer equation (eq. (3)) on quenching effect was used to determine K_{sv}. I_o and I are the fluorescence intensity before and after the addition of melamine, and [M] is the molar concentration of melamine. The Stern-Volmer plot is shown in Figure 6b. K_{sv} is the quenching effect coefficient of the melamine [29].

$$\text{Limit of Detection (LOD)} = 3.3 \times (\sigma/s) \quad (1)$$

$$\text{Limit of Quantification(LOQ)} = 10 \times (\sigma/s) \quad (2)$$

$$Io/I = 1 + Ksv\,[M] \quad (3)$$

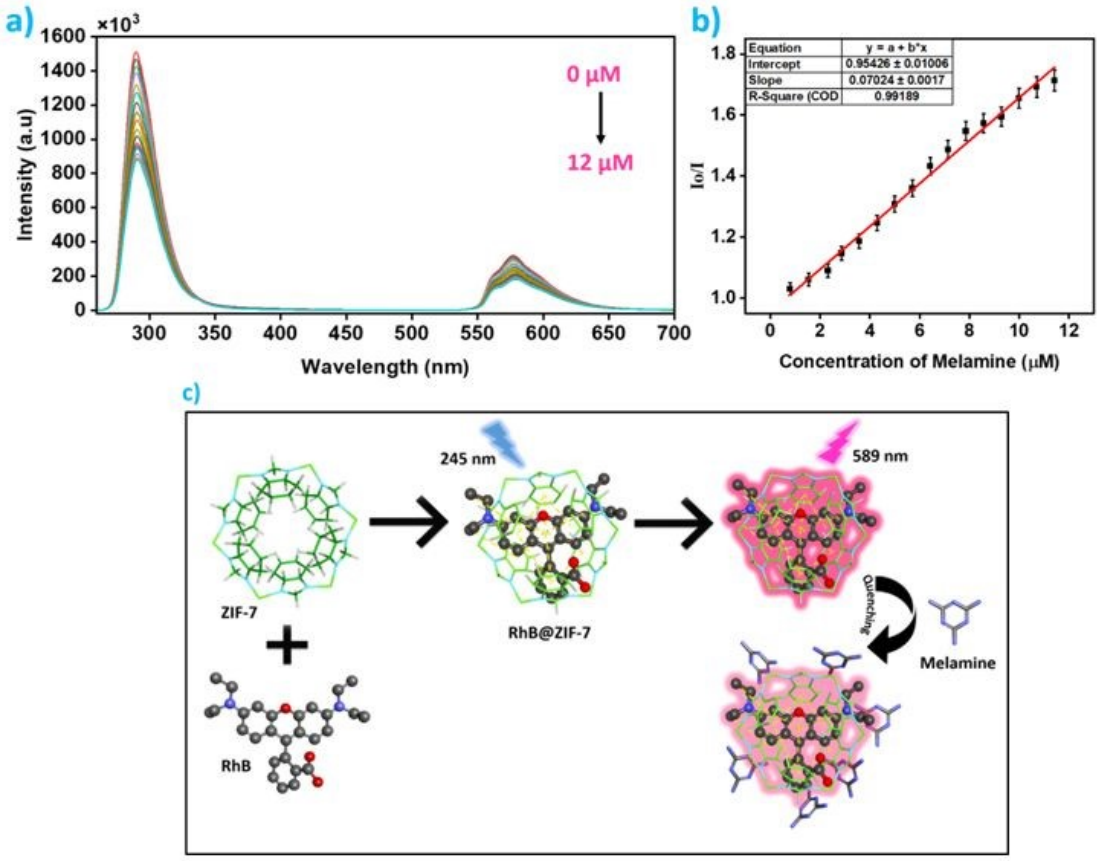

Figure 6. a) Fluorescence response of RhB_{30}@ZIF-7 with the addition of melamine. b) SV plot showing the variation of fluorescence intensity of RhB_{30}@ZIF-7 with melamine concentration. c) Schematic representation of fluorescence quenching on melamine addition.

View Article Online
DOI: 10.1039/D5NA00633C

Figure 6b shows a linear relationship between I_0/I and [M], concentration of melamine in the range of 0-12 μM (0-1.51 ppm) and $R^2 = 0.99$, confirming the suitability of this method for sensing. Further, analysis shows LOD for melamine as 0.47 μM (0.059 ppm) and LOQ as 1.4 μM (0.1766 ppm), which is lower than the safety limit of melamine that should be present in adult food and infant formulations, i.e., 2.5 ppm and 1 ppm, respectively. Comparison of the limit of detection achieved by various MOF composites for the optical sensing of melamine is tabulated in Table 1. Dual emissive MOF composite with dye encapsulation has not been explored yet, and the current work achieved an LOD value lower than the safety limit over a wide range of melamine concentrations.

Table 1: Comparison of detection performance of various MOF composites for melamine detection.

S No	Material	Detection Method	Tested matrix	Linear range	LOD (μM)	Ref
1	Ag-MOF@Fe/SnO_2	Colorimetric detection	Raw milk	39.6-198.0 μM	14.27	[27]
2	UiO-66-NH_2@Ru	Fluorescent sensing	Milk powder	0.27-110 μM	90×10^{-3}	[31]
3	$CsPbBr_3$/HZIF-8	Fluorescent sensing	Raw milk Infant formulation	3-500 × 10^{-3} μM	2.64×10^{-3}	[30]
4	CeO_2@NH_2-MIL(Fe)	Fluorescent biosensing	Milk Milk powder Protein beverage	0-0.05 μM	7.6×10^{-3}	[29]
5	CeO_2-MIL(Fe)	Colorimetric detection	Milk Milk powder	0-0.1 μM	8.0×10^{-3}	[28]
6	RhB_{30}@ZIF-7	Fluorescent detection	Infant formulation	0-12 μM	0.47 μM	This work

4.7. Mechanism for the detection of melamine with RhB_{30}@ZIF-7

Fluorescence response of dual emissive sensor based on RhB_{30}@ZIF-7 for melamine detection under the optimized conditions was studied (Figure 6c). The fluorescence emission

View Article Online
DOI: 10.1039/D5NA00633C

intensity at λ_{ex} = 271 nm gradually decreased with the increase of melamine concentration. The emissions at 290 nm and 578 nm corresponding to ZIF-7 and RhB, respectively, showed a quenching in response due to the addition of melamine in the concentration range of 0-15 μM. The XRD for recovered RhB_{30}@ZIF-7 - melamine complex shows no significant change, indicating non non-collapsed ZIF-7 skeleton after the sensing of melamine and supported by the UV-Visible absorption studies. Interestingly, Internal filtering effect (IFE) results in significant fluorescent quenching by competitive absorption of excited energy between the melamine and RhB_{30}@ZIF-7, or in some cases, through absorption of fluorescent emission of RhB_{30}@ZIF-7.

Here, the absorption of melamine was observed to be at 240 nm with a shoulder peak at 277 nm. The emission wavelength of RhB_{30}@ZIF-7 appears at 290 nm at an excitation wavelength of 271 nm (Figure S9). An overlap in the absorption spectra of melamine with the excitation wavelength of RhB_{30}@ZIF-7 was observed. The competitive absorption of the excitation wavelength of RhB_{30}@ZIF-7 by melamine reduces the fluorescent intensity in emission spectra. When the concentration of melamine increases, more energy is absorbed, resulting in the lower emission intensity of the RhB_{30}@ZIF-7 system in the presence of melamine. The IFE was dependent on the spectral overlap between the melamine and RhB_{30}@ZIF-7. Additionally, the specific functional groups (-OH and $–NH_2$) on the fluorescence sensing system RhB_{30}@ZIF-7 can alter the emission characteristics due to non-covalent interactions with melamine, thereby quenching fluorescence intensity. Further comparison on the lifetime decay analysis of RhB_{30}@ZIF-7 in the presence and absence of melamine is carried out (Figure 7). The lifetime before the addition of melamine and after melamine addition is found to be 6.6 ns. Absence of significant change in lifetime value for both samples also confirms the IFE as a sensing mechanism rather than any other mechanisms involving energy transfer between the sensing probe and the analyte[67].

4.8. Selectivity of the sensor

View Article Online
DOI: 10.1039/D5NA00633C

The selectivity is a key feature of an optical sensor in real-time applications. The interference studies were conducted in the presence of different potential interfering ions, and chemicals present in infant formulations were taken to ensure selectivity towards melamine. In the presence of K^+, Na^+, Mg^{2+}, Zn^{2+}, Mn^{2+}, Fe^{2+}, Ca^{2+}, glucose, lactose, glycine, lycine, and glutamic acid, high selectivity was observed for melamine, indicating RhB_{30}@ZIF-7 as a potential dual emissive fluorescence sensing probe for melamine detection (Figure S10).

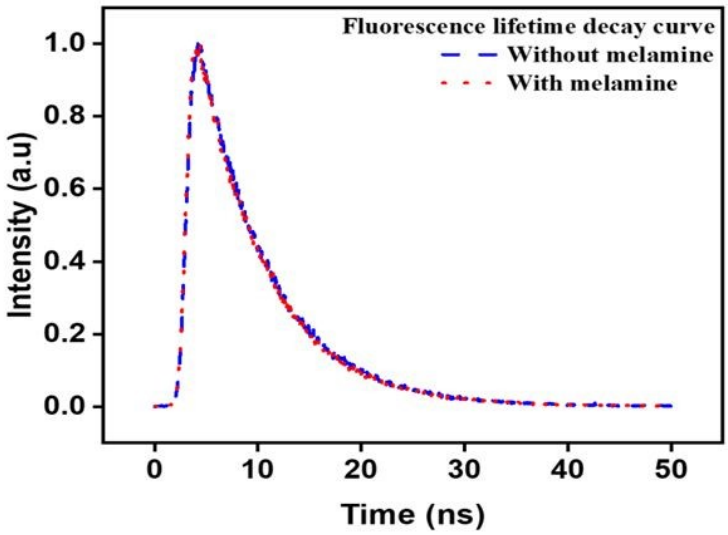

Figure 7. Lifetime decay comparison of RhB_{30}@ZIF-7 in the absence and presence of melamine.

5. Real sample analysis

5.1. Sample pre-treatment

2 g of infant formula powder was dissolved in 1.2 ml of CH_3COOH and 1.5 ml of $CHCl_3$. The solution was stirred and centrifuged for about 20 min to obtain a homogeneous suspension. The supernatant solution was collected and diluted with 1000 mL of milli-Q water, followed by centrifugation for 10 min at 3000 rpm while maintaining the pH at 7.0.

5.2. Analysis of unspiked and spiked samples

50 µl of 1 mg/ml RhB_{30}@ZIF-7, 2500 µl of pH 7.0 PBS, and 450 µl pre-treated infant formula solutions were added. This solution was kept for 10 min incubation at room temperature, and the fluorescence spectra of each sample were analysed at the optimized

View Article Online
DOI: 10.1039/D5NA00633C

conditions. Different concentration of melamine solutions was added separately into pre-treated infant formula samples along with RhB_{30}@ZIF-7, and a similar procedure was followed to detect the concentration of melamine.

5.3. Detection of melamine in infant formulations

To confirm the accuracy of RhB_{30}@ZIF-7 for sensing melamine in infant formulations standard addition method was adopted. The pre-treatment of infant formulation samples was done using the aforementioned method. The results indicated no detection of melamine in the unspiked infant formulation samples using the RhB_{30}@ZIF-7 sensor. The fluorescent detection exhibited a relative standard deviation (RSD%, n=5) of spiked infant formulation samples with melamine between 2.45% - 4.95% and recovery percentage was obtained between 99.00% - 106.5% indicating the accuracy of the method, suggesting reliable precision and reproducibility as shown in Table 2. The RSD values below 5% and the signal to noise ratio (SNR) analysis with an estimated SNR of 7 at 1μM melamine, and the corresponding increase with concentration, highlight the high repeatability and sensitive detection even at very low concentrations. The SNR is greater than 70 at 10μM, and its value across the evaluated concentration range indicates the stable signals obtained from the sensor with negligible background noise, thereby supporting the accuracy of the established linearity. All these results confirm the efficiency of RhB_{30}@ZIF-7 as a sensitive probe for melamine detection in a real sample matrix.

View Article Online
DOI: 10.1039/D5NA00633C

Table 2. Determination of melamine in infant formula samples using RhB_{30}@ZIF-7 fluorescent sensing platform.

Real samples	Added (μM)	Found (μM)	% Recovery (n=5)	RSD* (%)
Sample I[a]	0	ND	-	-
	1.0	1.01 ± 0.05	101.0	4.95
	2.0	2.13 ± 0.07	106.5	3.29
Sample I[b]	0	ND	-	-
	1.0	1.03 ± 0.04	103.0	3.88
	2.0	2.03 ± 0.07	101.5	3.45
Sample I[c]	0	ND	-	-
	1.0	0.99 ± 0.035	99.0	3.54
	2.0	2.04 ± 0.05	102.0	2.45
Sample I[d]	0	ND	-	-
	1.0	1.01 ± 0.035	101.0	3.47
	2.0	2.21 ± 0.07	110.5	3.17

*n=5 individual determination

$$\% \text{ Recovery} = \frac{\text{Found}}{\text{Added}} \times 100$$

I[a]; Amulspray, Gujarat Co-operative Milk Marketing Federation, Gujarat
I[b]; Lactogen Pro, Nestle India Limited, New Delhi
I[c] ; Zerolac, Raptakos, Brett & Co. LTD, Maharashtra
I[d]: Novel, British Life Sciences, Bangalore, Karnataka

6. Conclusion

A novel fluorescent sensing probe, RhB_{30}@ZIF-7, was synthesized by a one-pot solvothermal method via in situ encapsulation of RhB into ZIF-7 pores. The resulting RhB_{30}@ZIF-7 fluorescent system has dual emissions due to the two components present in it, ZIF-7 and RhB, which enabled the fluorescent detection of melamine in real infant formula samples. The fluorescent intensity decreased at 290 nm and 578 nm on melamine addition. The sensing system RhB_{30}@ZIF-7 showed a linear range between the concentration of melamine in the range of 0-12 μM, and the LOD of melamine is evaluated to be 0.47 μM and LOQ as

1.4 μM with R^2 of 0.99. RhB_{30}@ZIF-7 can be used for the detection of melamine in real infant formula samples with good recovery (99.75% - 101.5%) and RSD (2.50% - 4.95 %) values. While the present study establishes the feasibility of dye encapsulated fluorescein probe RhB_{30}@ZIF-7 for ultrasensitive detection of melamine, future works could focus on broadening the applicability of the probe towards selective detection of other nitrogen-rich adulterants in complex food matrices.

7. Ethics approval and consent to participate

Not applicable.

8. Consent for publication

Not applicable.

9. Availability of data and materials

The datasets generated and/or analysed during the current study are available from the corresponding author on reasonable request.

10. Funding

The authors greatly acknowledge the funding provided by the Centre for Research, CHRIST University, in the form of seed funding with Ref No.CU-ORS-SM-24/70.

11. CRediT authorship contribution statement

Sreevidhya K B: Investigation, Formal analysis, Methodology, writing – original draft, Suvardhan Kanchi: Conceptualization, Project administration, Writing – review & editing.

12. Declaration of Competing Interest

The authors declare that they have no known competing financial interests or personal relationships that could have appeared to influence the work reported in this paper.

13. Data availability

Data will be made available on request.

14. Acknowledgements

View Article Online
DOI: 10.1039/D5NA00633C

We sincerely thank Dr Abhijeet K Chaudhari for his valuable suggestions in synthesising the nanomaterials and their characterization.

References

1. J. R. Ingelfinger, *N Engl J Med*, 2008, **359**, 2745-2748.
2. R. A. Lynch, H. Hollen, D. L. Johnson and J. Bartels, *International Journal of Food Contamination*, 2015, **2**.
3. M. F. Neerman, W. Zhang, A. R. Parrish and E. E. Simanek, *Int J Pharm*, 2004, **281**, 129-132.
4. P. Goyal, P. Soppina, S. K. Misra, E. Valsami-Jones, V. Soppina and S. Chakraborty, *Front Toxicol*, 2022, **4**, 917749.
5. Y. C. Tyan, M. H. Yang, S. B. Jong, C. K. Wang and J. Shiea, *Anal Bioanal Chem*, 2009, **395**, 729-735.
6. S. Öztürk and N. Demir, *Journal of Food Composition and Analysis*, 2021, **100**, 103931.
7. W. Chansuvarn, S. Panich and A. Imyim, *Spectrochim Acta A Mol Biomol Spectrosc*, 2013, **113**, 154-158.
8. M. M. Deabes and R. El- Habib, *Journal of Environmental & Analytical Toxicology*, 2012, **02**.
9. E. W. P. Moore and F. Maya, *Nanomaterials (Basel)*, 2023, **13**.
10. H. Sun, L. Wang, L. Ai, S. Liang and H. Wu, *Food Control*, 2010, **21**, 686-691.
11. M. S. Filigenzi, B. Puschner, L. S. Aston and R. H. Poppenga, *J Agric Food Chem*, 2008, **56**, 7593-7599.
12. R. A. Yokley, L. C. Mayer, R. Rezaaiyan, M. E. Manuli and M. W. Cheung, *J Agric Food Chem*, 2000, **48**, 3352-3358.
13. J. P. Toth and P. C. Bardalaye, *J Chromatogr*, 1987, **408**, 335-340.
14. Y. Wen, H. Liu, P. Han, Y. Gao, F. Luan and X. Li, *J Sci Food Agric*, 2010, **90**, 2178-2182.
15. W. Yin, J. Liu, T. Zhang, W. Li, W. Liu, M. Meng, F. He, Y. Wan, C. Feng, S. Wang, X. Lu and R. Xi, *J Agric Food Chem*, 2010, **58**, 8152-8157.
16. F. Sun, L. Liu, H. Kuang and C. Xu, *Food and Agricultural Immunology*, 2013, **24**, 79-86.
17. E. Koglin, B. J. Kip and R. J. Meier, *The Journal of Physical Chemistry*, 1996, **100**, 5078-5089.
18. Z. Guo, Y.-t. Zhao, Y.-h. Li, T. Bao, T.-s. Sun, D.-d. Li, X.-k. Luo and H.-t. Fan, *Food Analytical Methods*, 2017, **11**, 546-555.
19. J. An, L. Li, Y. Ding, W. Hu, D. Duan, H. Lu, D. Ye, X. Zhu and H. Chen, *Electrochimica Acta*, 2019, **326**, 134946.
20. M. Alizadeh Sani, G. Jahed-Khaniki, A. Ehsani, N. Shariatifar, M. H. Dehghani, M. Hashemi, H. Hosseini, M. Abdollahi, S. Hassani, Z. Bayrami and D. J. McClements, *Biosensors (Basel)*, 2023, **13**.

21. M. Angelopoulou, P. Petrou and S. Kakabakos, *TrAC Trends in Analytical Chemistry*, 2024, **175**, 117714.
22. S. Oliveira, M. Sharifuzzaman, G. Moro, A. Sinibaldi, Z. Altintas, S. Kumar, F. Chiavaioli and C. Marques, *TrAC Trends in Analytical Chemistry*, 2025, **184**, 118139.
23. Z. Ling, L. Yang, W. Zhang, T. Yao and H. Xu, *Food Safety and Health*, 2024, **2**, 72-95.
24. M. Shellaiah and K. W. Sun, *Chemosensors*, 2019, **7**, 9.
25. Q. Xu, F. Xiao and H. Xu, *Trends Analyt Chem*, 2023, **161**, 116999.
26. Y. Zhao, H. Zeng, X. W. Zhu, W. Lu and D. Li, *Chem Soc Rev*, 2021, **50**, 4484-4513.
27. T. Shahzadi, H. Bibi, T. Riaz, M. Zaib and T. Malik, *Plasmonics*, 2024, DOI: 10.1007/s11468-024-02333-1.
28. A. Amalraj, M. Narayanan and P. Perumal, *Analyst*, 2022, **147**, 3234-3247.
29. A. Amalraj and P. Perumal, *New Journal of Chemistry*, 2022, **46**, 12952-12967.
30. S. Ahmed, S. Lahkar, S. Doley, D. Mohanta and S. Kumar Dolui, *Journal of Photochemistry and Photobiology A: Chemistry*, 2023, **443**, 114821.
31. C. Lin, C. Zhong, Y. Song and L. Wang, *Microchemical Journal*, 2021, **162**, 105837.
32. S. R. Venna and M. A. Carreon, *J Am Chem Soc*, 2010, **132**, 76-78.
33. K. S. Park, Z. Ni, A. P. Cote, J. Y. Choi, R. Huang, F. J. Uribe-Romo, H. K. Chae, M. O'Keeffe and O. M. Yaghi, *Proc Natl Acad Sci U S A*, 2006, **103**, 10186-10191.
34. X. C. Huang, Y. Y. Lin, J. P. Zhang and X. M. Chen, *Angew Chem Int Ed Engl*, 2006, **45**, 1557-1559.
35. Y. Zhu, X. Sun, Y. Tang, L. Fu and Y. Lu, *Nano Research*, 2020, **14**, 1912-1936.
36. X. Huang, J. Zhang and X. Chen, *Chinese Science Bulletin*, 2003, **48**, 1531-1534.
37. M. J. Dong, M. Zhao, S. Ou, C. Zou and C. D. Wu, *Angew Chem Int Ed Engl*, 2014, **53**, 1575-1579.
38. H.-R. Fu, L.-B. Yan, N.-T. Wu, L.-F. Ma and S.-Q. Zang, *Journal of Materials Chemistry A*, 2018, **6**, 9183-9191.
39. S.-J. Qin and B. Yan, *Sensors and Actuators B: Chemical*, 2018, **272**, 510-517.
40. J. Yoo, U. Ryu, W. Kwon and K. M. Choi, *Sensors and Actuators B: Chemical*, 2019, **283**, 426-433.
41. H. Zhao, J. Ni, J. J. Zhang, S. Q. Liu, Y. J. Sun, H. Zhou, Y. Q. Li and C. Y. Duan, *Chem Sci*, 2018, **9**, 2918-2926.
42. J. Wang, Y. Zhang, Y. Yu, F. Ye, Z. Feng, Z. Huang, X. Liu and X. Zhou, *Optical Materials*, 2019, **89**, 209-213.
43. Y. Tang, W. He, Y. Lu, J. Fielden, X. Xiang and D. Yan, *The Journal of Physical Chemistry C*, 2014, **118**, 25365-25373.
44. Z. Sun, A. Khurshid, M. Sohail, W. Qiu, D. Cao and S. J. Su, *Nanomaterials (Basel)*, 2021, **11**.
45. M. J. Snare, F. E. Treloar, K. P. Ghiggino and P. J. Thistlethwaite, *Journal of Photochemistry*, 1982, **18**, 335-346.
46. R. Sjöback, J. Nygren and M. Kubista, *Spectrochimica Acta Part A: Molecular and Biomolecular Spectroscopy*, 1995, **51**, L7-L21.

View Article Online
DOI: 10.1039/D5NA00633C

47. Y. Zhang, M. Gutierrez, A. K. Chaudhari and J. C. Tan, *ACS Appl Mater Interfaces*, 2020, **12**, 37477-37488.
48. A. K. Chaudhari and J. C. Tan, *Advanced Optical Materials*, 2020, **8**.
49. R. Xu, Y. Wang, X. Duan, K. Lu, D. Micheroni, A. Hu and W. Lin, *J Am Chem Soc*, 2016, **138**, 2158-2161.
50. C. He, K. Lu and W. Lin, *J Am Chem Soc*, 2014, **136**, 12253-12256.
51. M. Gutierrez, Y. Zhang and J. C. Tan, *Chem Rev*, 2022, **122**, 10438-10483.
52. Y. Zhang and J. C. Tan, *iScience*, 2021, **24**, 103035.
53. L. Yang, Y. L. Liu, C. G. Liu, Y. Fu and F. Ye, *RSC Adv*, 2020, **10**, 19149-19156.
54. J. Hassanzadeh, H. A. J. Al Lawati and I. Al Lawati, *Anal Chem*, 2019, **91**, 10631-10639.
55. D. A. Sherman, M. Gutiérrez, I. Griffiths, S. Mollick, N. Amin, A. Douhal and J. C. Tan, *Advanced Functional Materials*, 2023, **33**.
56. J. P. Zheng, S. Ou, M. Zhao and C. D. Wu, *Chempluschem*, 2016, **81**, 758-763.
57. Y. Gao, Y. Qi, K. Zhao, Q. Wen, J. Shen, L. Qiu and W. Mou, *Sensors and Actuators B: Chemical*, 2018, **257**, 553-560.
58. K. Kamali, S. Prasad, M. K. Sahoo, J. N. Behera, U. V. Waghmare and C. Narayana, *Inorg Chem*, 2022, **61**, 11571-11580.
59. K. Kamali, B. Joseph and C. Narayana, *Journal of Solid State Chemistry*, 2022, **309**, 122973.
60. X. Wang, M. Song and Y. Long, *Journal of Solid State Chemistry*, 2001, **156**, 325-330.
61. A. Davoodi, K. Akhbari and M. Alirezvani, *CrystEngComm*, 2023, **25**, 3931-3942.
62. K. Kim, K. J. Lopez, H.-J. Sun, J.-C. An, G. Park and J. Shim, *Journal of Applied Electrochemistry*, 2018, **48**, 1231-1241.
63. A. Arami-Niya, G. Birkett, Z. Zhu and T. E. Rufford, *J. Mater. Chem. A*, 2017, **5**, 21389-21399.
64. C. Cuadrado-Collados, J. Fernández-Català, F. Fauth, Y. Q. Cheng, L. L. Daemen, A. J. Ramirez-Cuesta and J. Silvestre-Albero, *Journal of Materials Chemistry A*, 2017, **5**, 20938-20946.
65. Y. Du, B. Wooler, M. Nines, P. Kortunov, C. S. Paur, J. Zengel, S. C. Weston and P. I. Ravikovitch, *Journal of the American Chemical Society*, 2015, **137**, 13603-13611.
66. M. Gustafsson and X. Zou, *Journal of Porous Materials*, 2013, **20**, 55-63.
67. S. Kumar Panigrahi and A. Kumar Mishra, *Journal of Photochemistry and Photobiology C: Photochemistry Reviews*, 2019, **41**, 100318.

View Article Online
DOI: 10.1039/D5NA00633C

A hierarchically porous RhB encapsulated ZIF-7 as a dual emission fluorescence probe for ultrasensitive detection of melamine in infant formulations

Sreevidhya K B, Suvardhan Kanchi*

*Department of Chemistry, CHRIST University, Bengaluru 560029, India
*Centre for Renewable Energy and Environmental Sustainability, CHRIST University, Bengaluru 560 029, India

Data Availability Statement

The data supporting this article have been included as part of the Supplementary Information.